TU Delft

Delft University of Technology

A Thrust-Elevator Interaction Criterion for Aircraft Optimal Longitudinal Control

Varriale, Carmine; Hameeteman, Kevin; Voskuijl, Mark; Veldhuis, Leo

DOI
10.2514/6.2019-3001

Publication date
2019

Document Version
Final published version

Published in
AIAA AVIATION Forum, 17-21 June 2019, Dallas, Texas

Citation (APA)
Varriale, C., Hameeteman, K., Voskuijl, M., & Veldhuis, L. (2019). A Thrust-Elevator Interaction Criterion for Aircraft Optimal Longitudinal Control. In *AIAA AVIATION Forum, 17-21 June 2019, Dallas, Texas* Article AIAA-2019-3001 American Institute of Aeronautics and Astronautics Inc. (AIAA). https://doi.org/10.2514/6.2019-3001

Important note
To cite this publication, please use the final published version (if applicable).
Please check the document version above.

Copyright
Other than for strictly personal use, it is not permitted to download, forward or distribute the text or part of it, without the consent of the author(s) and/or copyright holder(s), unless the work is under an open content license such as Creative Commons.

Takedown policy
Please contact us and provide details if you believe this document breaches copyrights.
We will remove access to the work immediately and investigate your claim.

This work is downloaded from Delft University of Technology.
For technical reasons the number of authors shown on this cover page is limited to a maximum of 10.

AIAA AVIATION Forum
17-21 June 2019, Dallas, Texas
AIAA Aviation 2019 Forum

10.2514/6.2019-3001

Check for updates

A Thrust-Elevator Interaction Criterion for Aircraft Optimal Longitudinal Control

Carmine Varriale*, Kevin Hameeteman†
Delft University of Technology, Delft, 2629 HS, The Netherlands

Mark Voskuijl‡
Netherlands Defence Academy, Den Helder, 1780 CA, The Netherlands

Leo L. M. Veldhuis§
Delft University of Technology, Delft, 2629 HS, The Netherlands

Downloaded by TU DELFT on July 11, 2019 | http://arc.aiaa.org | DOI: 10.2514/6.2019-3001

The aim of this research is to investigate the combined use of throttle and aerodynamic control vanes for aircraft optimal control. A new disruptive aircraft configuration concept is presented, featuring control vanes downstream of two rear-mounted ducted propellers. The aerodynamic interaction between the horizontal vane and the throttle is analyzed in the scope of a longitudinal control study. A static criterion is proposed to discern the efficiency of the interaction, with respect to a generic pitch command. A traditional control allocation logic is used to exploit the throttle as a secondary pitch effector, and a modified version based on the interaction criterion is proposed; its behavior is tested through an open-loop design space exploration of actuator time constants and effectors prioritization weights. A flexible control system architecture is designed to compare the aircraft closed-loop response in conjunction with a phugoid damper loop. Results show that the best tracking performance is obtained with pilot commands allocated to the elevator, and phugoid damper commands to both elevator and throttle. The traditional allocation method achieves the best tracking performance at the expense of the largest control effort. The modified allocation alleviates the effort while still achieving better performance than the non-coupled control.

Nomenclature

α	=	angle of attack, rad	I_{yy}	=	moment of inertia about y axis, kg $\cdot$ m^2
δ_e	=	elevator deflection, rad	M	=	pitch moment, N$\cdot$m
δ_T	=	normalized throttle	M_{δ_e}	=	pitch moment derivative w.r.t. δ_e, N$\cdot$m$\cdot$rad^{-1}
δ_p	=	normalized pilot stick command	M_{δ_T}	=	pitch moment derivative w.r.t. δ_T, N$\cdot$m
τ	=	first-order system time constant, s	S	=	wing area, m^2
Δ	=	variation with respect to trim condition	T	=	available thrust, N
c	=	mean aerodynamic chord, m	V	=	airspeed, m$\cdot$s^{-1}
q	=	pitch rate, rad$\cdot$s^{-1}	X, Z	=	forces in body axes, N
q_∞	=	free-stream dynamic pressure, Pa	$i, 0$	=	subscripts for initial condition
t	=	time, s	f, F	=	subscripts for final condition
u	=	generic control input	w, t, f	=	subscripts for wing, tail, fuselage
x, y, z	=	body axes reference frame	cmd	=	superscript for commanded value
x_T, z_T	=	thrust application point in body axes, m	tr	=	superscript for trim condition
B	=	control effectiveness matrix	$\mathcal{A}$	=	superscript for aerodynamic effects
C	=	non-dimensional coefficient	$\mathcal{P}$	=	superscript for propulsive effects

*Ph.D. Candidate, Flight Performance and Propulsion Section, Faculty of Aerospace Engineering, C.Varriale@tudelft.nl; AIAA Member.
†M.Sc. Student, Flight Performance and Propulsion Section, Faculty of Aerospace Engineering.
‡Full Professor, Faculty of Military Sciences, M.Voskuijl@mindef.nl; AIAA Member.
§Full Professor, Flight Performance and Propulsion Section, Faculty of Aerospace Engineering; AIAA Member.

Copyright © 2019 by Carmine Varriale, Kevin Hameeteman, Mark Voskuijl, Leo L. M. Veldhuis. Published by the American Institute of Aeronautics and Astronautics, Inc., with permission.

I. Introduction

The tremendous growth of the commercial transport aviation sector and the ever more stringent constraints on emissions and noise output have pushed aircraft designers to explore advanced solutions for more efficient and sustainable aircraft configurations. A disruptive conceptual design called DUUC (Delft University Unconventional Configuration) is presented in this paper from a flight control perspective. Its characteristic feature is the unconventional tail empennage, with horizontal and vertical control vanes mounted downstream of two ducted propellers, and spanning across their whole diameter. With this highly integrated architecture, referred to as the *propulsive empennage*, the DUUC tail synthesizes thrust, stability and control capabilities, allowing for clean wing aerodynamics (Fig 1). Integrating the tail surfaces with the propulsion system also has the potential to decrease the overall weight of the empennage, as compared to more conventional clean wing configurations like the T-tail with tail mounted engines.

For both jet and propeller engines with thrust vectoring control vanes, the control moment generated by the vanes not only depends on their deflection angle, but also on the jet stream velocity, and therefore on thrust. This tight interaction between the effectors (vanes and throttle) has been object of several research studies in the past. A method for including effectors aerodynamic interactions in a control problem has been presented in [1]. The interaction is included by augmenting the control effectiveness matrix B with second order derivatives terms. The non-linear problem is then solved with an iterative linear programming algorithm and results are shown for a re-entry vehicle equipped with rotatable nozzles. The rudder-propeller interaction problem is presented in [2, 3] for low speed marine applications: differently from the airborne case, craft motion is confined to a horizontal plane and rudders are effective only with forward thrust, making the generalized attainable moment set non-convex. A broad static wind tunnel test campaign has been conducted in [4] to analyse a ducted propeller with a vertical exit vane configuration. Jet engines for transonic applications have been investigated in static aerodynamic tests for various vanes designs and configurations. Experiments involving different convergent-divergent nozzle shapes [5, 6], an aircraft scaled model [7] and a full-scale research fighter [8] allowed to develop models for thrust loss and flow turning angle due to vanes deflections. More recently, a numerical and experimental study has been carried out in [9] to characterize the aerodynamic performance of a missile shroud equipped with four jet vanes. An experimental and numerical study on the isolated DUUC propulsive empennage has been presented in [10].

This paper focuses on investigating whether aero-propulsive interaction can be exploited to improve the aircraft control performance. After a brief presentation of the DUUC aircraft model in Sec. II, an interaction criterion for optimal longitudinal control is proposed in Sec. III. The interaction criterion is valid for different propulsive empennage configurations, as long as the jet stream at the duct outlet alters the control effectiveness of the vanes. Also, it is applicable to a wide range of aircraft configurations, as it is suitable for any engine position with respect to the aircraft Center of Gravity (CG). In Sec. IV, such criterion is integrated in a Control Allocation (CA) logic, and an open-loop performance index is proposed to estimate its benefit in terms of control power. Finally, in Sec. V, the CA logic is implemented in a variable architecture Flight Control System (FCS) and the classic RMSE index is considered for evaluating the closed-loop tracking performance.

II. Aircraft Model

The aircraft model consists of a conventional fuselage and wing, with the innovative propulsive empennage taking the place of the classic horizontal and vertical tails. The generic wing-body shape is based on the Boeing B737-700; the propulsive empennage is sized for stability with constraints on drag, and verified for control. The airfoil for both the empennage circular duct and the pylon is a NACA 0012, while the control vanes are designed with a NACA 0016 airfoil. The pylon is a straight untapered wing. The engine center body is a combination of a cylinder and ellipsoid shapes. The key aircraft characteristics are reported in Table 1. Mass and inertia have been estimated with statistical data, available for the B737-700, and semi-empirical models for the propulsive empennage [11, 12]. The geometry for the empennage has been realized in the ParaPy parametric software environment [13]. Figure 2 shows the body reference frame and the empennage geometry schematics as modeled in ParaPy.

The aerodynamic model has been obtained by means of CFD simulations with the Ansys Fluent workbench, using a steady inviscid Euler solver. As the scope of the present study is limited to longitudinal dynamics, the fluid domain has been assumed symmetric and only half of the aircraft model has been meshed. The propeller has been modeled as an actuator disk. The maximum available thrust per engine $T_{\max}$ is based on the performance of the F568-1 propeller, installed in the PW127 turboprop engine and mounted on the ATR72-600 [15], and is equal to 22 kN at sea level. The numerical dataset has been augmented with a semi-empirical drag correction model, based on the flat-plate skin-friction drag coefficient and the form factor method by [16]. The final aerodynamic dataset consists of the dimensionless forces

Downloaded by TU DELFT on July 11, 2019 | http://arc.aiaa.org | DOI: 10.2514/6.2019-3001

Downloaded by TU DELFT on July 11, 2019 | http://arc.aiaa.org | DOI: 10.2514/6.2019-3001

Table 1 DUUC geometric and inertial characteristics, as represented in Fig. 2.

Symbol	Value	Unit	Description
b	34.3	m	Wing span
c	3.96	m	Mean aerodynamic chord
l	34.5	m	Fuselage length
S	103.5	m^2	Wing area
r_{duct}	2.27	m	Empennage duct radius
c_{duct}	2.27	m	Empennage duct chord lenght
ϕ_{cb}	30.0	deg	Empennage cant angle
x_T	−10.75	m	Thrust application point coord. along x axis
z_T	−1.98	m	Thrust application point coord. along z axis
m	38.1 $\cdot 10^3$	kg	Aircraft mass
I_{yy}	1.88 $\cdot 10^6$	$kg \cdot m^2$	Moment of inertia about y axis

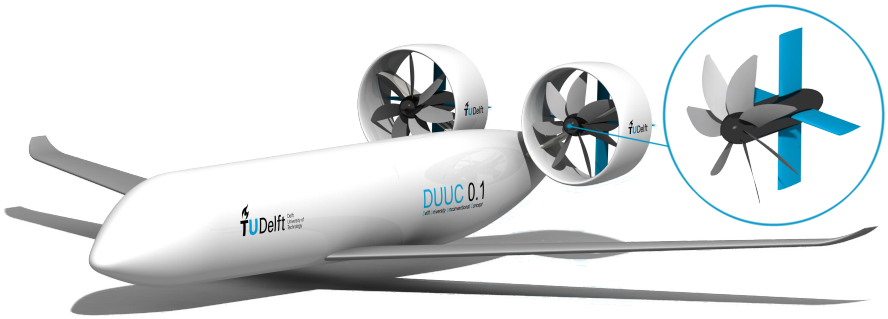

Fig. 1 DUUC aircraft concept with detail of its propulsive empennage [14].

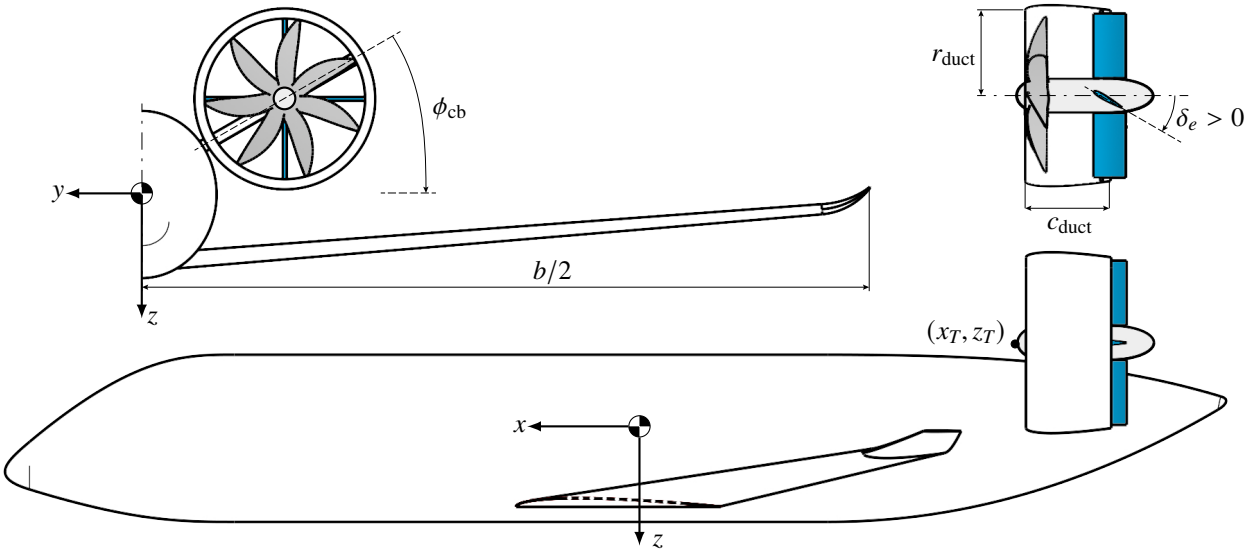

Fig. 2 DUUC geometry with body reference frame. Elevator deflection is positive as depicted.

C_X, C_Z and moment C_M in body axes, expressed as a function of α, δ_e and T.

The contributions of the three main aircraft parts (wing, fuselage and tail) are obtained separately and implemented as such in the in-house Performance, Handling Qualities and Loads Analysis Toolbox (PHALANX) [17]. This modular MATLAB®/Simulink toolbox integrates sub-models from different disciplines of aeronautics, in order to perform non-linear flight dynamics simulations. The toolbox has already been used in a variety of research studies to investigate the flight mechanics of novel aircraft configurations [18–21] and sub-scale aircraft designs [22]. The fidelity of each sub-model depends on available data, while the time domain simulations are driven by the Simscape Multibody Dynamics core. Within this framework, each of the aforementioned aircraft parts is modeled as a separate component: it is assigned a position and orientation with respect to an inertial reference frame, and rigidly connected to the other parts to form the aircraft assembly as a whole. Local flight parameters, such as α and V, can be measured at run time with this approach. By linking each component to its corresponding aerodynamic data set, every aircraft part generates its own aerodynamic actions from its own position relative to the aircraft CG. In this way, it is possible to exploit the difference in local speed and incidence to artificially generate unsteady aerodynamic effects like, for example, the tail damping due to aircraft pitch rate. As the CFD simulation is not time-dependent, these effects have to be interpreted as quasi-steady.

The FCS module features a fixed-gearing line to transmit pilot commands directly to the effectors (throttle and elevator), avoiding the use of any additional control logic: this is used to trim the aircraft model at specified flight conditions. Several trim methods are available, in the form of different optimization problem formulations. For the current application, the aircraft is set in straight and level flight, and the throttle and elevator deployed to trim for speed and pitch attitude, respectively. An unconstrained line-search algorithm with boundary check for effectors saturation has proved sufficient in this case. A parallel control line has been developed for both Open-Loop (OL) and Closed-Loop (CL) simulations. It models the FCS with a Non-linear Dynamic Inversion (NDI) approach and a CA algorithm, within a flexible control system architecture. For the inversion of motion dynamics, an analytic expression of the aerodynamic model is needed. For this reason, the aerodynamic data set of the separate aircraft parts has been synthesized in the following way:

$$\begin{gathered} C_X = C_{X,\mathrm{w}} + C_{X,\mathrm{t}}\frac{S_\mathrm{t}}{S} + C_{X,\mathrm{f}}\frac{S_\mathrm{f}}{S}; \qquad C_Z = C_{Z,\mathrm{w}} + C_{Z,\mathrm{t}}\frac{S_\mathrm{t}}{S} + C_{Z,\mathrm{f}}\frac{S_\mathrm{f}}{S} \\ C_M = C_{M,\mathrm{w}} + C_{M,\mathrm{t}}\frac{S_\mathrm{t}c_\mathrm{t}}{Sc} + C_{M,\mathrm{f}}\frac{S_\mathrm{f}c_\mathrm{f}}{Sc} + \sum_{i=\mathrm{w,t,f}}\left[C_{X,i}\frac{S_i\,(z_i - z_\mathrm{CG})}{Sc} - C_{Z,i}\frac{S_i\,(x_i - x_\mathrm{CG})}{Sc}\right] \end{gathered} \tag{1}$$

III. Aero-propulsive interaction model

The pitch moment coefficient can be generally expressed as the sum of two non-linear contributions, one due to direct propulsive actions and the other to pure aerodynamic actions:

$$C_M = C_M^{\mathcal{P}} + C_M^{\mathcal{A}}. \tag{2}$$

With reference to Fig. 3, the propulsive contribution to pitch moment can be modeled as

$$C_M^{\mathcal{P}} = C_M^{\mathcal{P}}(\alpha, \delta_e, \delta_T) = \frac{T}{q_\infty S}\frac{z_T}{c}\, f_T(\alpha, \delta_e, \delta_T)\,, \tag{3}$$

where the generic non-linear term accounts for out-of-axis conditions of the air stream at the engine inlet and thrust line rotation due to control vanes deflection. The term *elevator* – and hence the subscript e – is used to indicate the main effector devoted to pitch control; in case of the DUUC, this identifies with the horizontal control vane. For the sake of this work, no specific model needs to be formulated for the aerodynamic contribution. The following generic, non-linear function can be adopted:

$$\begin{gathered} C_M^{\mathcal{A}} = C_M^{\mathcal{A}}(\alpha, \delta_e, \delta_T) \\ \text{with} \quad C_{M_{\delta_e}}^{\mathcal{A}} = C_{M_{\delta_e}}^{\mathcal{A}}(\alpha, \delta_e, \delta_T) \quad \text{and} \quad C_{M_{\delta_T}}^{\mathcal{A}} = C_{M_{\delta_T}}^{\mathcal{A}}(\alpha, \delta_e, \delta_T)\,. \end{gathered} \tag{4}$$

For conventional aircraft configurations, which do not feature a significant thrust-elevator interaction, Eqs. 3 and 4 can be simplified in the following way:

Downloaded by TU DELFT on July 11, 2019 | http://arc.aiaa.org | DOI: 10.2514/6.2019-3001

$$C_M^{\mathcal{P}}(\alpha,\delta_e,\delta_T) \xrightarrow{\text{no interaction}} C_M^{\mathcal{P}}(\alpha,\delta_T) \tag{5a}$$

$$C_{M_{\delta_e}}^{\mathcal{A}}(\alpha,\delta_e,\delta_T) \xrightarrow{\text{no interaction}} C_{M_{\delta_e}}^{\mathcal{A}}(\alpha,\delta_e) \tag{5b}$$

$$C_{M_{\delta_T}}^{\mathcal{A}}(\alpha,\delta_e,\delta_T) \xrightarrow{\text{no interaction}} 0 \tag{5c}$$

In the remainder of this article, a trailing-edge-down deflection of the elevator is conventionally regarded as positive (Fig. 2), while a pitch-down moment is instead regarded as negative. With such a convention, the elevator control effectiveness is negative for all aircraft configurations with a rear empennage, i.e. whenever the elevator is aft of the aircraft CG.

$$C_{M_{\delta_e}} < 0 \tag{6}$$

Note that the lack of superscript implies the sum of the propulsive and aerodynamic contributions, i.e.:

$$C_{M_{\delta_e}} = C_{M_{\delta_e}}^{\mathcal{P}} + C_{M_{\delta_e}}^{\mathcal{A}} \quad \text{and} \quad C_{M_{\delta_T}} = C_{M_{\delta_T}}^{\mathcal{P}} + C_{M_{\delta_T}}^{\mathcal{A}} \tag{7}$$

We here define *concordant* the elevator and throttle actions that result in the same pitching tendency of the aircraft. For example, a pitch-down maneuver is initiated by the pilot with $\delta_e - \delta_e^{\text{tr}} > 0$; for those flight conditions for which $C_{M_{\delta_T}} < 0$, an increase in thrust also causes a pitch-down tendency of the aircraft. In these cases, therefore, a $\delta_T - \delta_T^{\text{tr}} > 0$ shift (throttle-up) is said to be concordant with the pilot's elevator maneuver. An engine throttle-down, instead, would be said to be *discordant* with the elevator maneuver, as it would cause a pitch-up tendency of the aircraft that opposes the original intention of the pilot. This definition is applicable to all aircraft configurations, with or without effectors interaction, and is expressed by the following static *concordance criterion*:

$$\left(\delta_e - \delta_e^{\text{tr}}\right) C_{M_{\delta_T}} < 0. \tag{8}$$

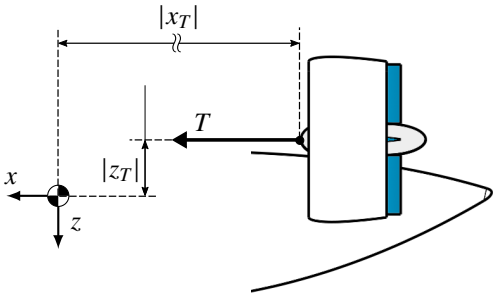

Fig. 3 Schematic of pitch moment contribution due to direct propulsive effects, $C_M^{\mathcal{P}}$.

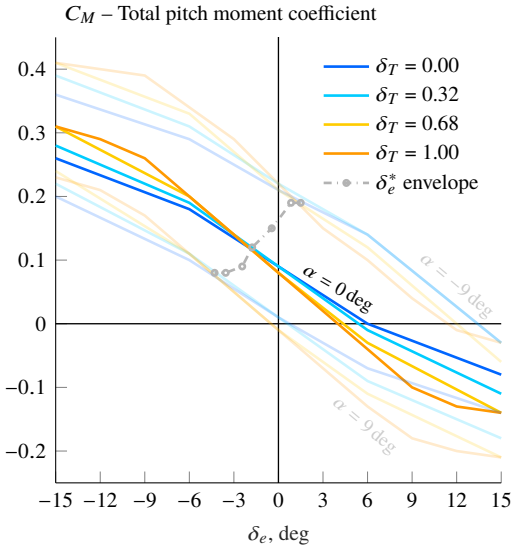

Fig. 4 Total pitch moment coefficient C_M for the DUUC. CFD simulations at $V = 80\,\text{m/s}$.

For configurations with negligible effectors interaction, Eqs. 3, 5a and 5c suggest that compliance with the concordance criterion depends only on the propulsive system vertical position with respect to the aircraft CG. If the propulsive system lies above the CG ($z_T < 0$), a throttle-up is always concordant with an elevator pitch-down maneuver; likewise for a throttle-down and elevator pitch-up combination. In case of relevant aero-propulsive interaction between the effectors, a variation in thrust determines a variation of the elevator control effectiveness. Increasing thrust makes the slope of each $C_M(\delta_e)$ curve more negative, as shown in Fig. 4. Also, for a certain range of angles of attack, an elevator deflection δ_e^* exists for which the pitch moment does not change with thrust. An increase in thrust results in a pitch-up tendency if $\delta_e < \delta_e^*$, while in a pitch-down tendency if $\delta_e > \delta_e^*$. This condition is represented in Fig. 4 with the gray line and defined by

$$\begin{cases} C_{M_{\delta_T}} > 0, & \delta_e < \delta_e^* \\ C_{M_{\delta_T}} = 0, & \delta_e = \delta_e^* \\ C_{M_{\delta_T}} < 0, & \delta_e > \delta_e^*. \end{cases} \tag{9}$$

Such definition allows the concordance criterion to be formulated in terms of notable elevator deflection values:

$$\begin{cases} \delta_e > \delta_e^*, & \delta_e > \delta_e^{\text{tr}} \\ \delta_e < \delta_e^*, & \delta_e < \delta_e^{\text{tr}}. \end{cases} \tag{10}$$

It can be seen in Fig. 4 that δ_e^* is negative at high angles of attack, while it becomes positive at the most negative incidences. The trim elevator deflection δ_e^{tr} is always more positive than δ_e^*, at any angle of attack and throttle setting.

Downloaded by TU DELFT on July 11, 2019 | http://arc.aiaa.org | DOI: 10.2514/6.2019-3001

The difference between the two decreases with increasing angle of attack and throttle setting. Finally, in case of an aircraft configuration with negligible aero-propulsive interaction, δ_e^* would be undefined.

In an attempt to characterize the effectors interaction for a propulsive empennage, and to discern whether the unconventional use of the throttle as a secondary pitch effector can be beneficial, the concordance criterion is further elaborated in the following subsections. Particular attention is placed on the throttle-up maneuver since, for a propulsive empennage, it always augments the elevator effectiveness $C_{M_{\delta_e}}$, regardless of its deflection δ_e (Fig. 4).

A. Aerodynamic thrust effectiveness

Moving from Eq. 3 and assuming that the thrust line remains parallel to the longitudinal body axis in all flight conditions, the pitch moment coefficient due to propulsive actions can be simply expressed as

$$C_M^{\mathcal{P}} = \frac{T}{q_\infty S}\frac{z_T}{c} = C_T \bar{z}_T. \tag{11}$$

The effects of high angle of attack at the engine inlet and the thrust vectoring capabilities of the control vanes are then both neglected. While the first is a strong assumption for some flight conditions, the second is surely acceptable for subsonic applications. Equation 11 leads then to:

$$C_{M_{\delta_e}}^{\mathcal{P}} = 0 \quad \Longrightarrow \quad C_{M_{\delta_e}} = C_{M_{\delta_e}}^{\mathcal{A}} \tag{12}$$

which also simplifies the notation. By making use of Eq. 11 and the definition of normalized throttle command

$$\delta_T = \frac{T - T_{\min}}{T_{\max} - T_{\min}} = \frac{T}{T_{\max}}, \tag{13}$$

the criterion in Eq. 8 becomes

$$\left(\delta_e - \delta_e^{\text{tr}}\right)\left(C_{T_{\max}}\bar{z}_T + C_{M_{\delta_T}}^{\mathcal{A}}\right) < 0 \tag{14}$$

or equivalently

$$\begin{cases} C_{M_{\delta_T}}^{\mathcal{A}} < -C_{T_{\max}}\bar{z}_T, & \delta_e > \delta_e^{\text{tr}} \\ C_{M_{\delta_T}}^{\mathcal{A}} > -C_{T_{\max}}\bar{z}_T, & \delta_e < \delta_e^{\text{tr}} \end{cases} \tag{15}$$

This formulation is referred to as the first-order concordance criterion. It involves the pitch thrust control derivative, i.e. the first-order derivative of pitch moment with respect to throttle command. This formulation does not require any additional model for $C_{M_{\delta_T}}^{\mathcal{A}}$ and is visualized in Fig. 5a, where three regions of interaction are highlighted. In all regions, a throttle-up command exerts a pitch-down propulsive action, due to the high-engine configuration.

In the green region ($\mathbb{G}$), the elevator exerts a pitch-down action on the aircraft. In this case, a throttle-up command is fully concordant with it: both the propulsive and aerodynamic actions of thrust are concordant with the aerodynamic action of the elevator. In the red ($\mathbb{R}$) and yellow ($\mathbb{Y}$) regions, the elevator aims at pitching the aircraft up. Therefore, the thrust propulsive action is discordant with the elevator's aerodynamic one. In the red region, because of the small magnitude of δ_e in this region, the thrust aerodynamic action (i.e. the increase in elevator effectiveness) is overcome by the thrust propulsive action. Throttling-up to increment the elevator effectiveness results in this case in a net decrease of control power. In the yellow region, due to the greater amplitude of δ_e, the thrust aerodynamic action overcomes the propulsive one, gaining a positive net benefit from the increase in elevator effectiveness. The control power in the commanded direction, therefore, increases overall.

If the aero-propulsive interaction can be neglected, the $C_{M_{\delta_T}}^{\mathcal{A}}(\delta_e)$ curve reduces to a horizontal line of value 0, according to Eq. 5c. This represents the very straightforward fact for which a high-mounted conventional engine is only concordant with pitch-down elevator maneuvers, while a low-mounted conventional engine is only concordant with pitch-up elevator maneuvers. In other words, in case of no throttle-elevator interaction, the yellow area in Fig. 5a is completely replaced by the red area. As a final observation, it can be seen in Fig. 5a that the non-linear thrust aerodynamic effectiveness curve manifests a stall behavior for $\delta_e = \pm 12°$. For $|\delta_e| > 12°$ increasing thrust no longer increases the elevator control effectiveness and the collaboration criterion has to be reformulated. This can be interpreted as the control reversal of the integrated pitch effector (combined elevator and throttle).

Downloaded by TU DELFT on July 11, 2019 | http://arc.aiaa.org | DOI: 10.2514/6.2019-3001

B. Second-order mixed effectiveness

As shown in Fig. 5a, the thrust aerodynamic effectiveness presents a reasonably linear behavior in a certain range of elevator deflections. Using Taylor's expansion, the following affine expression can be adopted for it

$$C^{\mathcal{A}}_{M_{\delta_T}} = C^{\mathcal{A}}_{M_{\delta_T}}(\alpha, \delta_e, \delta_T) \approx C^{\mathcal{A}}_{M_{\delta_T}}\left(\alpha, \delta_e^{\text{tr}}, \delta_T\right) + \left.\frac{\partial C^{\mathcal{A}}_{M_{\delta_T}}}{\partial \delta_e}\right|_{\delta_e^{\text{tr}}} \left(\delta_e - \delta_e^{\text{tr}}\right) \tag{16}$$

and re-written using a simpler notation:

$$C^{\mathcal{A}}_{M_{\delta_T}} \approx C^{\mathcal{A},\text{tr}}_{M_{\delta_T}} + C^{\text{tr}}_{M_{\delta\delta}} \left(\delta_e - \delta_e^{\text{tr}}\right), \qquad \text{with } C^{\text{tr}}_{M_{\delta\delta}} = \left.\frac{\partial C^{\mathcal{A}}_{M_{\delta_T}}}{\partial \delta_e}\right|_{\delta_e^{\text{tr}}}. \tag{17}$$

The quantity $C_{M_{\delta\delta}}$ is the second-order derivative of the pitch moment with respect to both the effectors, and is referred to as *mixed effectiveness*. As of the way it has been introduced, it represents the variation of thrust effectiveness with elevator deflection. Schwartz's theorem

$$C_{M_{\delta\delta}} = \frac{\partial C^{\mathcal{A}}_{M_{\delta_T}}}{\partial \delta_e} = \frac{\partial C^{\mathcal{A}}_{M_{\delta_e}}}{\partial \delta_T} \tag{18}$$

makes it more intuitive to interpret it as the variation of elevator effectiveness due to thrust. By substituting Eq. 17 in Eq. 14, the second-order concordance criterion is obtained

$$\Delta\delta_e \left(C_{T_{\max}} \overline{z}_T + C^{\mathcal{A},\text{tr}}_{M_{\delta_T}} + C^{\text{tr}}_{M_{\delta\delta}} \Delta\delta_e\right) < 0 \tag{19}$$

and reduced to the following single inequality:

$$C^{\text{tr}}_{M_{\delta\delta}} < -\frac{C_{T_{\max}} \overline{z}_T + C^{\mathcal{A},\text{tr}}_{M_{\delta_T}}}{\delta_e - \delta_e^{\text{tr}}}, \quad \delta_e \neq \delta_e^{\text{tr}}. \tag{20}$$

The three regions of interaction described before are recognizable again in Fig. 5b. Also, the same simplification for the case of no interaction applies. For the stalled values of δ_e, visible in Fig. 5a, the non-linear $C_{M_{\delta\delta}}$ curve does not respect the second order collaboration condition. The numeric values are positive and fall above the constraint hyperbola. For the same deflections, the non-linear curve for $C^{\mathcal{A}}_{M_{\delta_T}}$ does instead respect the first-order concordance criterion. This is not a contradiction, but a consequence of the linearity assumption made with Eq. 16, from which the second-order criterion is derived.

A key fact that has been used so far is Eq. 6, i.e. the negative sign of the elevator control effectiveness for rear empennage configurations. In the following section, the horizontal distance between the empennage and the CG is included explicitly in the formulation of the interaction model. This will also allow to extend the criterion to aircraft configurations with a front empennage.

C. Empennage horizontal position and vertical position

Figure 6 shows that the relation between the aerodynamic elevator effectiveness and thrust is close to linear for the whole range of throttle positions. Following a classic aerodynamic modeling approach, it can be written as

$$C^{\mathcal{A}}_{M_{\delta_e}} = C^{\mathcal{A}}_{M_{\delta_e}}(\alpha, \delta_e, \delta_T) \approx C^{\mathcal{A}}_{M_{\delta_e,0}}(\alpha, \delta_e) + \eta_{\text{t}} \frac{x_T}{c} C_{L_{\alpha,\text{t}}} \delta_T, \qquad \text{with} \quad \eta_{\text{t}} = \frac{q_{\infty,\text{t}}}{q_\infty} \frac{k S_{\text{t}}}{S} \tag{21}$$

where $C^{\mathcal{A}}_{M_{\delta_e,0}}$ is the elevator effectiveness for $\delta_T = 0$, and k is a scaling coefficient for the effective tail surface S_t. By differentiating with respect to δ_T and using again Eqs. 12 and 18, a simple expression is found for the mixed effectiveness

$$C_{M_{\delta\delta}} = \eta_{\text{t}} \frac{x_T}{c} C_{L_{\alpha,\text{t}}} = \eta_{\text{t}} \overline{x}_T C_{L_{\alpha,\text{t}}} \tag{22}$$

which then does not depend on the effectors' positions. With this assumption, the elevator effectiveness and the mixed effectiveness have the same sign as x_T, which is negative for a rear empennage. The second order concordance criterion

Downloaded by TU DELFT on July 11, 2019 | http://arc.aiaa.org | DOI: 10.2514/6.2019-3001

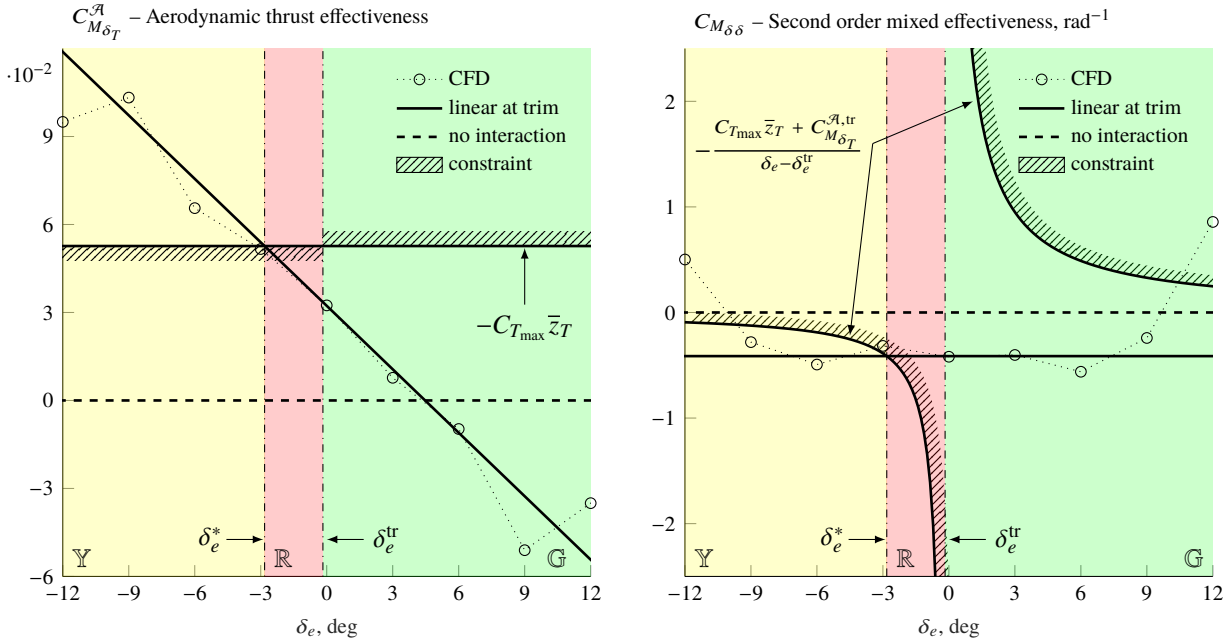

a) First-order concordance criterion

b) Second-order concordance criterion

Fig. 5 Concordance criteria for the DUUC. The case of a generic configuration with no thrust-elevator interaction is also presented. Trim conditions at sea level: $V^{\text{tr}} = 80\,\text{m/s}$, $\alpha^{\text{tr}} = 6.7°$, $\delta_e^{\text{tr}} = -0.2°$, $\delta_T^{\text{tr}} = 0.43$. Static margin = 10%.

of Eq. 20 can now be re-written in terms of both the horizontal and vertical position of the empennage, by using Eq. 22:

$$\begin{cases} \Delta\delta_e > -\dfrac{C_{T_{\max}}\bar{z}_T + C^{\mathcal{A},\text{tr}}_{M_{\delta_T}}}{\eta_t C_{L_{\alpha,t}}\bar{x}_T}, & \Delta\delta_e > 0 \\ \Delta\delta_e < -\dfrac{C_{T_{\max}}\bar{z}_T + C^{\mathcal{A},\text{tr}}_{M_{\delta_T}}}{\eta_t C_{L_{\alpha,t}}\bar{x}_T}, & \Delta\delta_e < 0. \end{cases} \tag{23}$$

This formulation is suited for an interesting geometric interpretation, which can be visualized in Fig. 7. The equation associated with these inequalities represents the following bundle of lines in the (x, z) plane:

$$\ell\,(\Delta\delta_e):\ C_{T_{\max}}\frac{z}{c} = -\eta_t C_{L_{\alpha,t}}\left(\delta_e - \delta_e^{\text{tr}}\right)\frac{x}{c} - C^{\mathcal{A},\text{tr}}_{M_{\delta_T}}. \tag{24}$$

Each line belonging to it has the following properties:

- at the aircraft CG longitudinal position, $x = 0$, the vertical distance to the CG is equal to $-cC^{\mathcal{A},\text{tr}}_{M_{\delta_T}}/C_{T_{\max}}$;
- the slope follows the horizontal vane deflection relative to trim conditions, and in particular:
  - for $\delta_e = \delta_e^{\text{tr}}$, the line is parallel to the longitudinal body axis;
  - for $\delta_e > \delta_e^{\text{tr}}$, the line goes through quadrants $\mathbb{II}$ and $\mathbb{IV}$, i.e. from below the aircraft tail to above its nose;
  - for $\delta_e < \delta_e^{\text{tr}}$, the line goes through quadrants $\mathbb{I}$ and $\mathbb{III}$, i.e. from above the aircraft tail to below its nose;
- the right hand side of Eq. 23 locates the line passing through the thrust application point, indicated with ℓ_T.

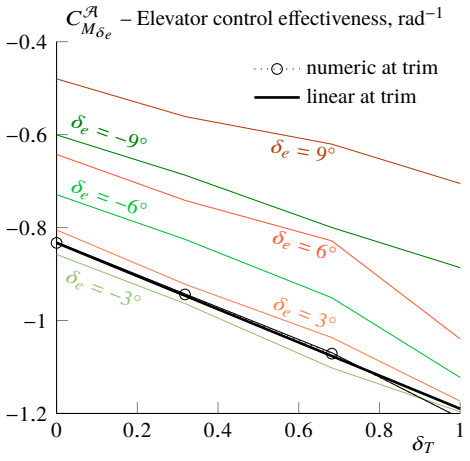

Fig. 6 Accuracy of linear model for the elevator control effectiveness. Trim conditions as in Fig. 5, $q_t/q_\infty = 1$, $k = 0.12$.

Downloaded by TU DELFT on July 11, 2019 | http://arc.aiaa.org | DOI: 10.2514/6.2019-3001

For any relative deflection of the elevator, a line ℓ from Eq. 24 can be drawn on the chart. For $\delta_e > \delta_e^{\text{tr}}$, the throttle action is beneficial for the pitch maneuver if ℓ falls below ℓ_T in the tail region. For $\delta_e < \delta_e^{\text{tr}}$, the throttle action is beneficial for the pitch maneuver if ℓ falls above ℓ_T in the tail region.

By comparing these results with the previous formulations of the concordance criterion, it is clear that

$$\Delta\delta_e^* = -\frac{C_{T_{\max}}\bar{z}_T + C_{M_{\delta_T}}^{\mathcal{A},\text{tr}}}{\eta_t C_{L_{\alpha,t}}\bar{x}_T} \quad \Longrightarrow \quad \delta_e^* = \delta_e^{\text{tr}} - \frac{C_{T_{\max}}\bar{z}_T + C_{M_{\delta_T}}^{\mathcal{A},\text{tr}}}{\eta_t C_{L_{\alpha,t}}\bar{x}_T} \tag{25}$$

and the line of the bundle passing through the engine location is represented by

$$\ell_T : \; z = -\frac{\eta_t C_{L_{\alpha,t}}}{C_{T_{\max}}}\Delta\delta_e^* x - c\frac{C_{M_{\delta_T}}^{\mathcal{A},\text{tr}}}{C_{T_{\max}}}. \tag{26}$$

Equation 23 reduces to the explicit form of the original concordance criterion in Eq. 10:

$$\begin{cases} \Delta\delta_e > \Delta\delta_e^*, & \Delta\delta_e > 0 \\ \Delta\delta_e < \Delta\delta_e^*, & \Delta\delta_e < 0 \end{cases} \iff \begin{cases} \delta_e > \delta_e^*, & \delta_e > \delta_e^{\text{tr}} \\ \delta_e < \delta_e^*, & \delta_e < \delta_e^{\text{tr}}, \end{cases} \tag{27}$$

but an analytic expression for δ_e^* is now available in terms of geometric and trim parameters.

D. Extension to under-the-wing engine configurations

The concordance criteria derived in the preceding sections can be adapted to aircraft configurations with any kind of engine empennage fore of the aircraft CG. In such a case, a positive deflection of the elevator determines a pitch-up tendency of the aircraft and Eq. 6 no longer holds true. For front empennage configurations ($x_T > 0$),

$$C_{M_{\delta_e}} > 0 \tag{28}$$

and the concordance criterion has to be stated as

$$\left(\delta_e - \delta_e^{\text{tr}}\right) C_{M_{\delta_T}} > 0. \tag{29}$$

With the same assumptions adopted for the previous formulations, the latter equation can be expanded to the following first- and second-order concordance criteria for aircraft configurations with engines in front of the CG:

$$\begin{cases} C_{M_{\delta_T}}^{\mathcal{A}} > -C_{T_{\max}}\bar{z}_T, & \delta_e > \delta_e^{\text{tr}} \\ C_{M_{\delta_T}}^{\mathcal{A}} < -C_{T_{\max}}\bar{z}_T, & \delta_e < \delta_e^{\text{tr}} \end{cases}; \qquad C_{M_{\delta\delta}}^{\text{tr}} > -\frac{C_{T_{\max}}\bar{z}_T + C_{M_{\delta_T}}^{\mathcal{A},\text{tr}}}{\delta_e - \delta_e^{\text{tr}}}, \quad \delta_e \neq \delta_e^{\text{tr}} \tag{30}$$

These relations present inverted inequality signs with respect to their counterparts for rear empennages. The geometric interpretation remains unchanged from Eq. 23, and therefore can be interpreted as a natural extension of Fig. 7 to the $x > 0$ half-plane.

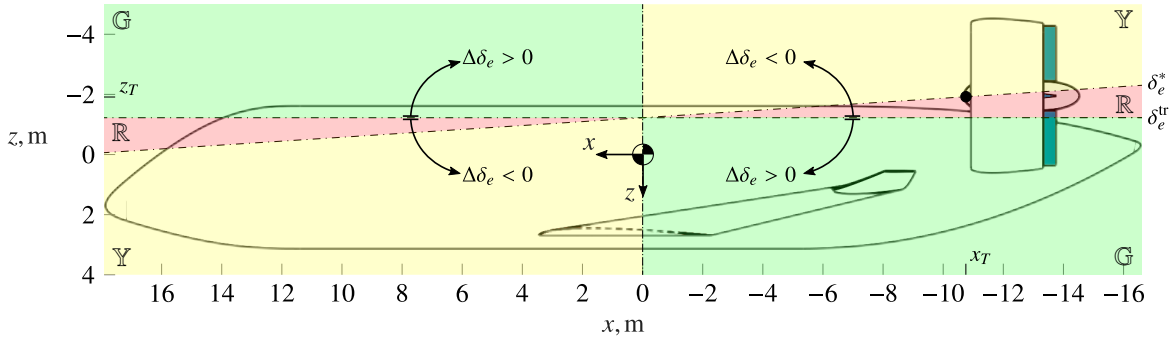

Fig. 7 Geometric interpretation of the concordance criterion. Trim conditions as in Fig. 5.

Downloaded by TU DELFT on July 11, 2019 | http://arc.aiaa.org | DOI: 10.2514/6.2019-3001

IV. Control Allocation Logic

The interaction model developed in the previous section is now applied to the design of a longitudinal control law. The aim is to investigate on the optimal control strategy for aircraft mounting a propulsive empennage. To do so, the throttle is included in the pitch control problem as an additional effector, and performance in terms of control power and tracking precision is compared to traditional control approaches. Exploiting the throttle-elevator interaction makes the aircraft system over-actuated and the control problem redundant. In other terms, the control effectiveness matrix B is not square and the equation for the pitch control problem

$$C_M^{\text{cmd}} = Bu \qquad \Longleftrightarrow \qquad C_M^{\text{cmd}} = \begin{bmatrix} C_{M_{\delta_e}} & C_{M_{\delta_T}} \end{bmatrix} \begin{Bmatrix} u_e \\ u_T \end{Bmatrix} \tag{31}$$

is under-determined in the unknown u, and therefore does not have a unique solution. The problem of distributing pilot (or autopilot) commands to multiple effectors consists in solving Eq. 31 for u, and is generally referred to as the CA problem [23]. Since the B matrix cannot be simply inverted, the CA problem is usually solved by means of optimization techniques.

For the present work, an Automatic Flight Control System (AFCS) has been designed for the DUUC, based on a NDI control law. The NDI approach allows to separate neatly the generation of control commands from the distribution of control effort. A high-level schematic of the AFCS is shown in Fig. 8. Actuators for both the elevator and the throttle are modeled as first order dynamic systems with saturation limits. The CA algorithm is based on the Weighted Pseudo Inverse (WPI) method, modified with a non-linear filter derived from the concordance criterion. The method allows for flexibility in the choice of an optimization criterion, and results in an analytic expression of the unknown control deflections, therefore having no convergence issues. The classic WPI CA matrix is obtained by solving the following quadratic programming problem

$$\min_u \frac{1}{2} \left\| W_u \left(u - u_{\text{d}} \right) \right\|^2 \qquad \text{s.t. } Bu - C_M^{\text{cmd}} = 0, \; u_{\min} \leq u \leq u_{\max} \tag{32}$$

and referred to as the minimum-norm, or Moore-Penrose, pseudo-inverse. The quantity u_{d} is a preferred arrangement of the effectors, such as the null deflection. W_u is a positive-definite matrix which penalizes the effectors on the basis of the value of their corresponding weight. Due to the simple problem formulation, the solution to Eq. 32 has an analytic form given by

$$u = u_d + \left[W_u^{-1} B^{\intercal} \left(B W_u^{-1} B^{\intercal} \right)^{-1} \right] \left(C_M^{\text{cmd}} - B u_{\text{d}} \right) = u_d + B^{\dagger} \left(C_M^{\text{cmd}} - B u_d \right), \tag{33}$$

where $B^{\dagger}$ is referred to as the WPI of B [24]. In the present work, the weighting matrix is chosen as:

$$W_u = \begin{bmatrix} 1 & 0 \\ 0 & W_T f_W \end{bmatrix} \tag{34}$$

where

$$f_W = f_W \left(\alpha, \delta_e, \delta_T, \delta_e^{\text{tr}} \right) = \max \left\{ 1, \; N \left(\delta_e - \delta_e^{\text{tr}} \right) C_{M_{\delta_T}} \right\} \quad \text{with} \quad N \gg 1. \tag{35}$$

The elevator is given an allocation weigh equal to 1, while the throttle weight is a function of the concordance criterion of Eq. 8. If the criterion is not satisfied, the throttle is assigned an allocation weight $W_u^{2,2} \approx N W_T$, which heavily penalizes it and therefore leaves it inactive during the maneuver. If the criterion is satisfied, the throttle weight is equal to W_T. A sensitivity study has been performed on the allocation algorithm behavior and on the effect of the non-linear filter, for different combinations of penalization coefficients W_T and thrust actuator speeds. The latter could be illustrative

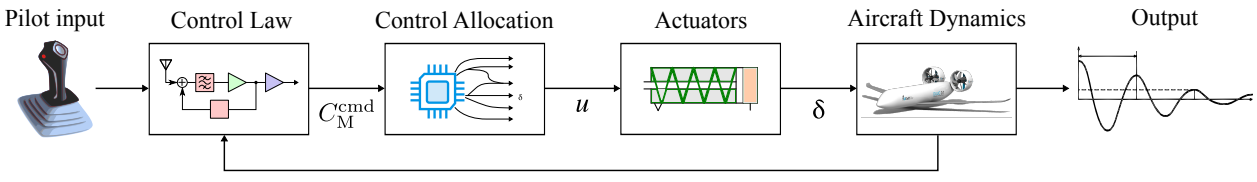

Fig. 8 Qualitative Flight Control System scheme.

Downloaded by TU DELFT on July 11, 2019 | http://arc.aiaa.org | DOI: 10.2514/6.2019-3001

of different mechanisms employed to control thrust, like the engine pressure ratio or the propeller blades pitch angle. The elevator actuator time constant is fixed at $\tau_e = 0.05\,\mathrm{s}$ and its position saturation limits at $\pm 30°$. The aircraft is commanded with a reference pitch-rate and its open-loop response is measured. A specified maneuver is simulated three times, each with different control allocation settings. These are labeled in the following way, for future reference:

E: with the elevator as the only active effector;
E+T/on: with the throttle available as an active effector and the non-linear allocation matrix as in Eq. 34;
E+T/off: with the throttle available as an active effector, but the linear allocation matrix, i.e. with $f_W \equiv 1$.

The time series from **E+T/on** and **E+T/off** are then compared to those from **E**, which is used as a reference case. The comparison is carried out with respect to the open-loop dimensionless performance index

$$P_{\mathrm{ol}} = \frac{\displaystyle\int_{t_i}^{t_f} \left(|q| - |q_{\mathrm{ref}}| \right) \mathrm{d}t}{\dfrac{1}{t_f - t_i} \displaystyle\int_{t_i}^{t_f} |\delta_T - \delta_T^{\mathrm{tr}}| \, \mathrm{d}t}, \tag{36}$$

which has been conceived to synthesize the benefit of extra control power – numerator – at the expense of extra control effort – denominator – in an open-loop simulation. The time instants t_i and t_f correspond to the start and end of the pilot input command. The integrand function at the numerator gives P_{ol} its sign. It is positive when the pitch rate response q overcomes the one obtained in the reference case, either during a pitch-down or a pitch-up maneuver; it is negative otherwise. A visualization of the integrand function is shown in Fig. 9. The denominator is always positive and measures the effort required to activate the additional effector. If no throttle command is used, P_{ol} is not defined. Such an index is easily adaptable to all dynamics problems involving coupling of axes, variable number of effectors and control system architectures. Results for an impulse and a 2-3-1-1 maneuver of various amplitudes are shown in Fig. 10.

For the impulse maneuver, some clear global trends are recognizable: the more aggressive the pitch-down maneuver, the more benefit is gained from the exploitation of the interaction. As expected, the faster the throttle actuator is, the higher the gain, although with decreasing rate of improvement. It is interesting to note that the slowest analyzed throttle actuator ($\tau_T/\tau_e = 100$) has a positive effect on the overall control power even in the case of full-stick pitch-up maneuver. Finally, the value of P_{ol} increases monotonically with the allocation weight W_T, up to a plateau. This indicates a threshold in throttle prioritization, no matter what its actuator time constant is. The non-linear allocation filter makes a small difference only in the pitch-up maneuver with high-prioritization of the throttle. Because of the way it is designed, using it or not in such a pitch-down maneuver results in the same throttle action.

For the 2-3-1-1 maneuver, due to the rapid change of the command and its switches in sign, the P_{ol} trend with respect to the command amplitude is lost, but the general characteristics of the algorithm still hold, and some more considerations can be made. For the saturated cases – outer lower charts – there is no clear P_{ol} plateau anymore. In case of a maneuver starting with a pitch-down command, the performance index has a local maximum at about $W_T = 0.1$; for a pitch-up initial command, instead, P_{ol} keeps increasing for $0.1 < W_T < 1$. For the non-saturated cases – inner lower charts – the two fastest throttle actuators do not improve the performance significantly, or even deteriorate it. The effect

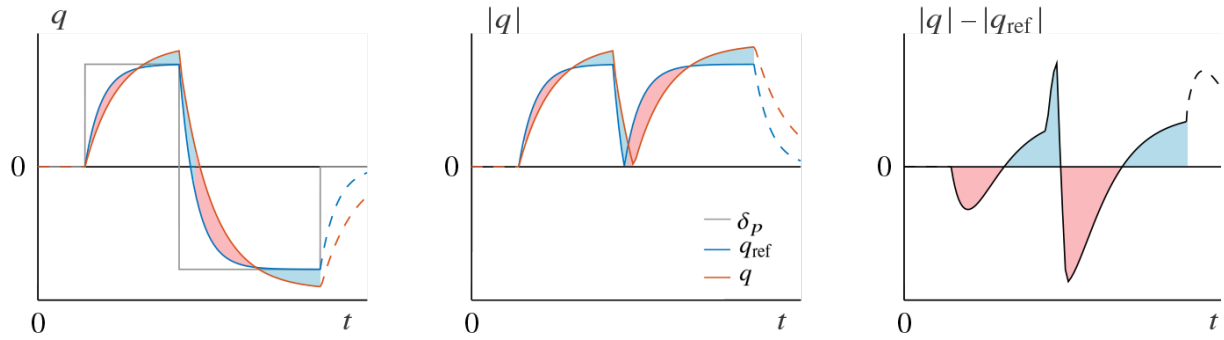

Fig. 9 Qualitative representation of the integrand function at the numerator of Eq. 36. The blue area represents a positive contribution to P_{ol}, while the red area a negative one. Such contribution is evaluated only during the pilot maneuver on the stick. Its sign does not depend on the sign of q and q_{ref}, but on the difference in magnitude between q and q_{ref}.

Downloaded by TU DELFT on July 11, 2019 | http://arc.aiaa.org | DOI: 10.2514/6.2019-3001

Downloaded by TU DELFT on July 11, 2019 | http://arc.aiaa.org | DOI: 10.2514/6.2019-3001

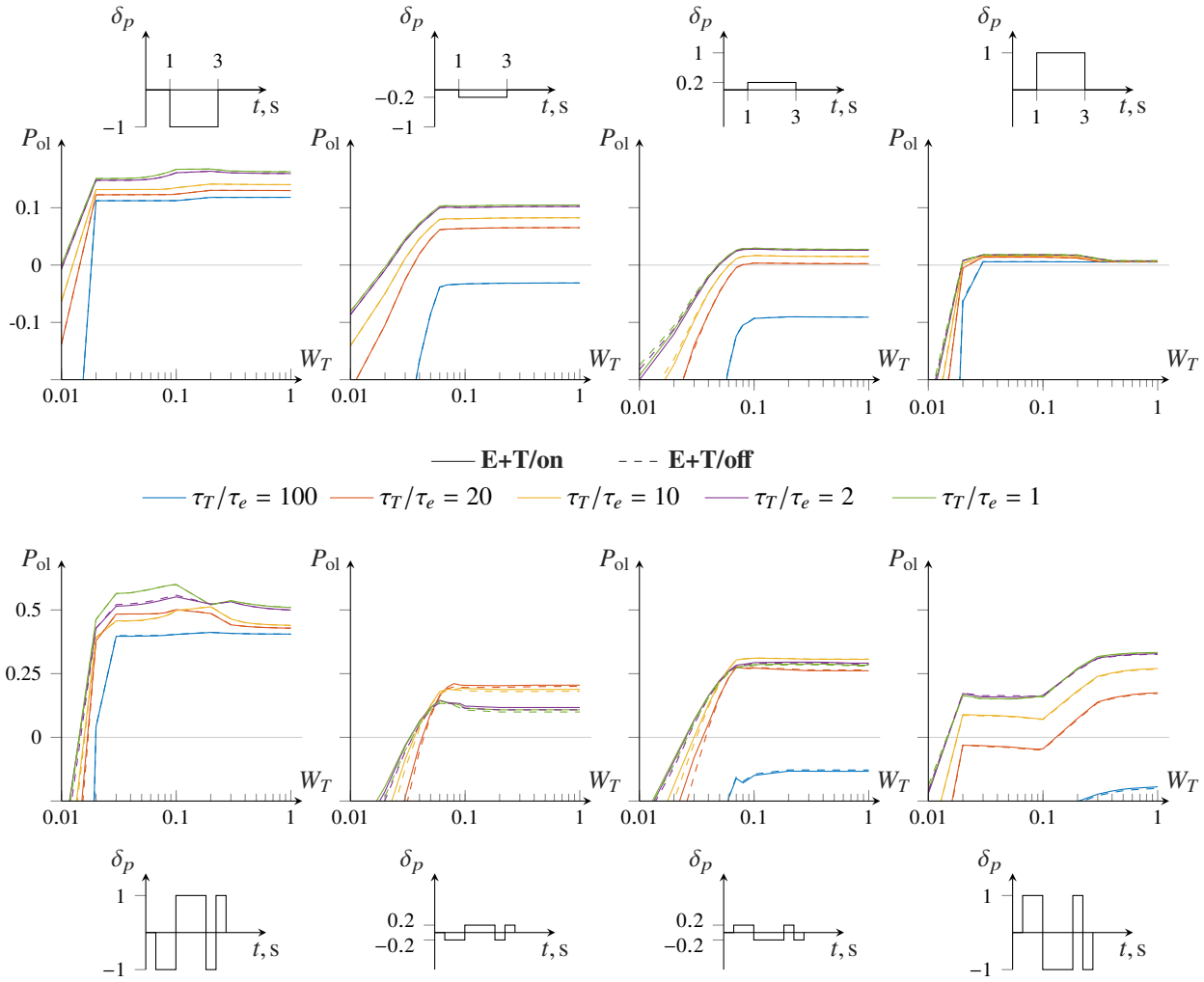

Fig. 10 Open-loop performance benefit as a function of thrust allocation weight W_T and non-linear allocation filter f_W. Elevator actuator speed $\tau_e = 0.05$ s. Trim conditions as in Fig. 5. (*Top row*) 2 s impulse maneuver. (*Bottom row*) 2-3-1-1 maneuver.

of the non-linear filter is more visible: it slightly increases the benefit in control power, the effect being greater for actuators with high prioritization (small W_T).

V. Closed-Loop Comparison

The primary role of thrust, on conventional configurations as well as on those mounting a propulsive empennage, is to ensure the control of aircraft airspeed. It has been shown in the previous section how thrust can also be used to control the aircraft pitch rate. The aim of this part of the work is to test the closed-loop performance of the proposed CA logic when it interacts with control loops that also involve thrust and elevator in the short period, such as a phugoid damper. In order to do so, the flexible control system architecture depicted in Fig. 11 has been developed. The control law is based on a pitch rate response type, and features a pitch damper and a phugoid damper loop. The latter generates a control signal on airspeed error, which arises from deviations in airspeed from the trim condition. The pitch damper is modeled with a PI + feed-through controller, while the phugoid damper is simply a PI controller. Both the loops can be opened and closed by switches. A distribution logic makes it possible to either merge the control output of the pitch and the phugoid dampers before the allocation, or keep them separate to be processed with different allocation methods. The NDI+CA block features control logics to allocate its input only to the elevator or also to the throttle, and to switch from the linear CA or the filtered CA algorithm. The pitch moment equation of motion is linearized in the controls and

written as

$$\dot{q} = \frac{q_\infty Sc}{I_{yy}} \Delta C_M = \frac{q_\infty Sc}{I_{yy}} Bu. \tag{37}$$

In the most general case, when both elevator and throttle are active effectors, it is inverted to obtain the following control allocation problem:

$$Bu = \begin{bmatrix} C_{M_{\delta_e}} & C_{M_{\delta_T}} \end{bmatrix} \begin{Bmatrix} u_e \\ u_T \end{Bmatrix} = \frac{I_{yy}\dot{q}}{q_\infty Sc} = C_M^{\text{cmd}} \tag{38}$$

where the control derivatives are calculated for the trim positions of the effectors, but are a non-linear function of the angle of attack. The PI controllers have been tuned to obtain a specified closed-loop performance with the AFCS architecture indicated as I in Table 2. In this case, used as reference for the comparison, the elevator is the only active effector and the pitch and phugoid damper control signal is merged before the allocation. Since only one effector is used for the control of the pitch moment, the allocation problem is not under-determined and Eq. 38 reduces to the simple division

$$Bu = C_{M_{\delta_e}} u_e = \frac{I_{yy}\dot{q}}{q_\infty Sc} = C_M^{\text{cmd}} \quad \Longrightarrow \quad u_e = \frac{C_M^{\text{cmd}}}{C_{M_{\delta_e}}}. \tag{39}$$

The time histories of airspeed and throttle are reported in Fig. 12 for two doublet and two 2-3-1-1 maneuvers. With controller gains considered frozen, the control loops and logics are systematically varied to obtain the remaining four AFCS architectures reported in Table 2. An allocation weight $W_T = 0.1$ is chosen, with actuators time constants for the elevator and throttle being $\tau_e = 0.05\,\text{s}$ and $\tau_T = 1\,\text{s}$, respectively. The RMS error (RMSE) of the commanded flight parameters V and q with respect to their reference signal is measured for the selected maneuvers. The pitch rate RMSE is not reported for it does not present any remarkable difference among the analyzed cases. The same holds for the elevator deflection time histories. The airspeed RMSE and the average throttle command effort

$$\overline{\Delta\delta}_T = \frac{1}{t_F - t_0} \int_{t_0}^{t_F} |\delta_T - \delta_T^{\text{tr}}| \, \mathrm{d}t \tag{40}$$

are also reported in the bar charts of Fig. 12. Equation 40 is very similar to the denominator on the right hand side of Eq. 36, but the time interval is now extended to the whole simulation length.

As it can be seen in the charts, AFCS architectures II and III do not produce a significative difference in the tracking performance of the airspeed. In these two cases, the phugoid and the pitch damper commands are merged, and their sum is allocated on both the elevator and throttle, with and without filtering logic, respectively. The time histories of δ_T show how the throttle command closely follows the pilot elevator command which characterizes the given maneuver, with a slight effort reduction for the filtered approach. On the other hand, AFCS architectures IV and V visibly improve the performance of the reference case. In these cases, the pilot and pitch damper command is allocated only on the elevator, while the phugoid damper on both the elevator and the throttle. The non-filtered allocation delivers the best results in terms of tracking performance, at the expense of maximum throttle usage. The filtered allocation (architecture IV) achieves a good compromise between tracking error and control effort; due to the filter non-linearity, though, the performance appears to be maneuver dependent and the time histories can show abrupt triggering of the CA logic, resulting possibly in undesired system behavior. For example, Figures 12a and 12c show sharp changes in the time history of δ_T during the pilot stick command, which could give rise to actuator wear. Figure 12d shows how the filtered allocation logic can also be triggered by the evolution of the flight condition, in case of no pilot commands on the stick. This is visible as a sudden drop in throttle command when the flight conditions for the verification of the concordance criterion are met; this strongly non-linear behavior could potentially be unpleasant for the pilot. Finally, in the same figure, the throttle time response for both architectures IV and V is shown not to revert back to its initial condition.

VI. Conclusion

The propulsive empennage concept has been presented with application to a new disruptive aircraft configuration. A generic model for the aerodynamic interaction between thrust and control vanes has been proposed. It has been shown how a throttle-up maneuver causes an increase in the control effectiveness of the vanes, and an analytic criterion for optimal longitudinal control has been formulated moving from this phenomenon. A non-trivial flight mechanical behavior has been shown to arise due to the effectors interaction, which clearly distinguishes the propulsive empennage from a conventional engine-tail configuration. A control allocation logic has been proposed, which exploits

Downloaded by TU DELFT on July 11, 2019 | http://arc.aiaa.org | DOI: 10.2514/6.2019-3001

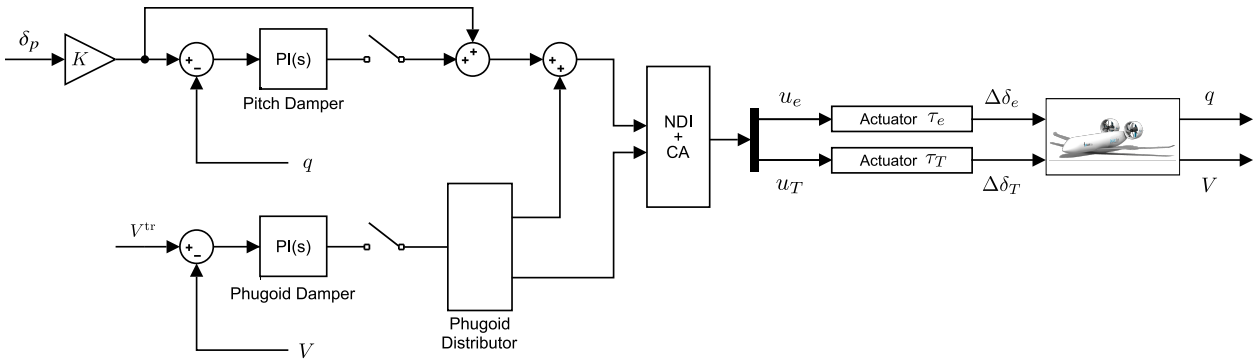

Fig. 11 Automatic Flight Control System with variable architecture.

Table 2 Description of tested Flight Control System architectures. Reference to Fig. 11

AFCS Architecture	Pitch Damper CA	Phugoid Distributor	Phugoid Damper CA
I	**E**	To Pitch Damper	**E**
II	**E+T/on**	To Pitch Damper	**E+T/on**
III	**E+T/off**	To Pitch Damper	**E+T/off**
IV	**E**	To NDI+CA	**E+T/on**
V	**E**	To NDI+CA	**E+T/off**

the aforementioned criterion, and a flight control system with variable architecture has been developed to test it in conjunction with a phugoid damper loop. The capability to track an airspeed reference depends on the control system architecture more than the capability to track a pitch rate reference. Exploiting the interaction for the phugoid damper gives the least tracking error, with the interaction criterion easing the required additional control effort.

Future work will focus on trim and static stability models for aircraft configurations featuring the propulsive empennage concept, and the formulation and implementation of a dynamic collaboration criterion that solves the undesired non-linear behavior of the current static one.

Acknowledgments

The authors thank Nando van Arnhem for the helpful information on the DUUC aircraft design, and Reinier van Dijk and his team at ParaPy B.V. for providing them with the ParaPy software libraries.

References

[1] Oppenheimer, M., and Doman, D., "A Method for Including Control Effector Interactions in the Control Allocation Problem," *AIAA Guidance, Navigation and Control Conference and Exhibit*, American Institute of Aeronautics and Astronautics, 2007. doi:10.2514/6.2007-6418.

[2] Johansen, T. A., Fuglseth, T. P., Tøndel, P., and Fossen, T. I., "Optimal constrained control allocation in marine surface vessels with rudders," *Control Engineering Practice*, Vol. 16, No. 4, 2008, pp. 457 – 464.

[3] Lindegaard, K. ., and Fossen, T. I., "Fuel-efficient rudder and propeller control allocation for marine craft: experiments with a model ship," *IEEE Transactions on Control Systems Technology*, Vol. 11, No. 6, 2003, pp. 850–862.

[4] Mort, K. W., and Gamse, B., "A Wind-Tunnel Investigation of a 7-foot-Diameter Ducted Propeller," Tech. rep., NASA Ames Research Center, 1967.

[5] Berrier, B. L., and Mason, M. L., "Static Performance of an Axisymmetric Nozzle With Post-Exit Vanes for Multiaxis Thrust Vectoring," Tech. rep., NASA Langley Research Center, 1988.

Downloaded by TU DELFT on July 11, 2019 | http://arc.aiaa.org | DOI: 10.2514/6.2019-3001

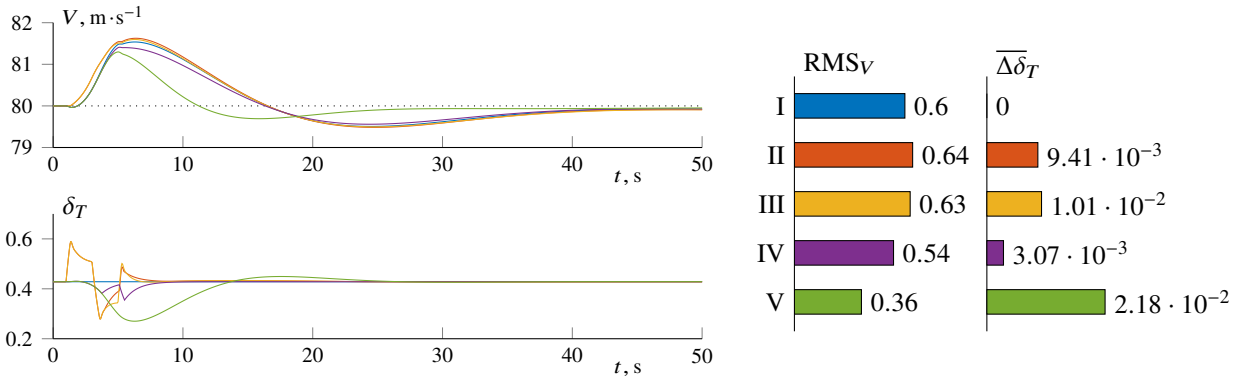

a) 2s doublet maneuver of amplitude **A** = **−0.1**.

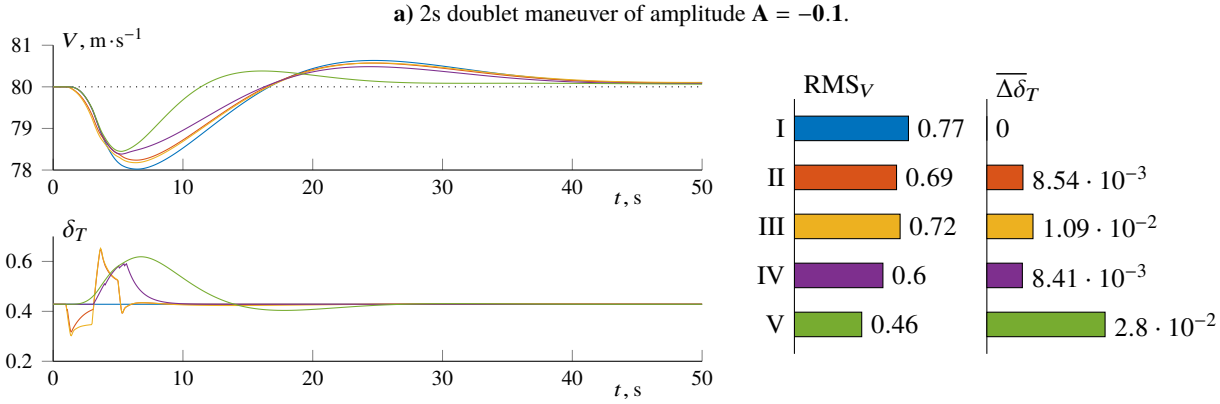

b) 2s doublet maneuver of amplitude **A** = **+0.1**.

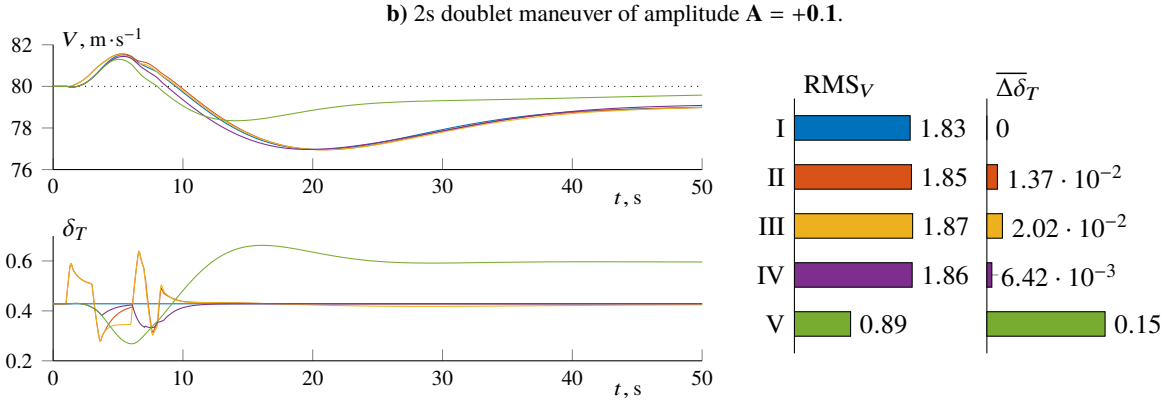

c) 2-3-1-1 maneuver of amplitude **A** = **−0.1**.

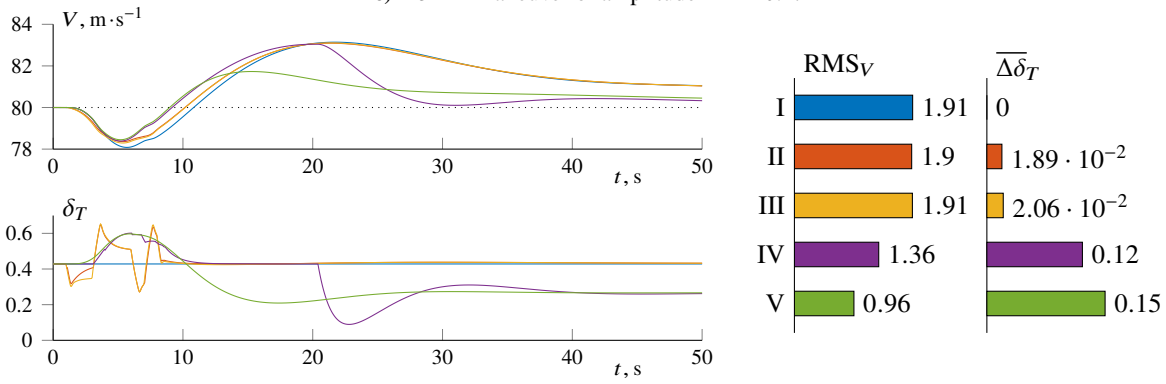

d) 2-3-1-1 maneuver of amplitude **A** = **+0.1**.

Fig. 12 Time histories of airspeed and throttle, airspeed RMSE and average throttle effort for various simulated maneuvers. Trim conditions as in Fig. 5. FCS architectures as in Table 2.

Downloaded by TU DELFT on July 11, 2019 | http://arc.aiaa.org | DOI: 10.2514/6.2019-3001

[6] Mason, M. L., and Berrier, B. L., "Static Performance of Nonaxisymmetric Nozzle With Yaw Thrust-Vectoring Vanes," Tech. rep., NASA Langley Research Center, 1988.

[7] Bowers, A. H., Noffz, G. K., Grafton, S. B., Mason, M. L., and Peron, L. R., "Multiaxis Thrust Vectoring Using Axisymmetric Nozzles and Postexit Vanes on an F/A-18 Configuration Vehicle," Tech. rep., NASA Dryden Flight Research Facility, 1991.

[8] Johnson, S. A., "Aircraft Ground Test and Subscale Model Results of Axial Thrust Loss Caused by Thrust Vectoring Using Turning Vanes," Tech. rep., NASA Dryden Flight Research Facility, 1992.

[9] Sung, H.-G., and Hwang, Y.-S., "Thrust-Vector Characteristics of Jet Vanes Arranged in X-Formation Within a Shroud," *Journal of Propulsion and Power*, Vol. 20, No. 3, 2004, pp. 501–508. doi:10.2514/1.10381.

[10] Harinarain, V. N., "Aerodynamic Performance Study on a Ducted Propeller System for Propulsion and Control & Stability Applications," Master's thesis, Delft University of Technology, 2017.

[11] Scheidler, S. G., "Mass Analysis - An Important Discipline of the "Luftfahrttechnisches Handbuch" (Aeronautical Engineering Handbook)," *71st Annual Conference, Bad Gögging, Germany*, 2012.

[12] Brady, C., *The Boeing 737 Technical Guide*, Tech Pilot Services Ltd, 2010.

[13] van Dijk, R., and Baan, M., "ParaPy B.V." , 2017. Available: https://www.parapy.nl/.

[14] van Arnhem, N., "DUUC aircraft with the innovative 'Propulsive Empennage' concept," Youtube, 2016. Available: `https://www.youtube.com/watch?v=VDbJBkcQBPI`.

[15] Filippone, A., *Advanced Aircraft Flight Performance*, Cambridge Aerospace Series, Cambridge University Press, 2012.

[16] Raymer, D. P., *Aircraft Design: A Conceptual Approach, Fifth Edition*, AIAA Education Series, AIAA, 2012.

[17] Voskuijl, M., La Rocca, G., and Dircken, F., "Controllability of Blended Wing Body Aircraft," *26th Congress of International Council of the Aeronautical Sciences*, 2008.

[18] Kok, E., Voskuijl, M., and van Tooren, M. J. L., "Distributed Propulsion featuring Boundary Layer Ingestion Engines for the Blended Wing Body Subsonic Transport," *6th AIAA Multidisciplinary Design Optimization Specialist Conference*, 2010.

[19] Prakasha, P., Ciampa, P. D., Della Vecchia, P., Ciliberti, D., Voskuijl, M., Charbonnier, D., Jungo, A., Zhang, M., Fioriti, M., Anisimov, K., and Mirzoyan, A., "Model Based Collaborative Design & Optimization of Blended Wing Body Aircraft Configuration: AGILE EU Project," *AIAA Aviation and Aeronautics Forum and Exposition*, 2018.

[20] Voskuijl, M., de Klerk, J., and van Ginneken, D., "Flight mechanics modelling of the Prandtl plane for conceptual and preliminary design." *Variational Analysis and Aerospace Engineering: Mathematical Challenges for Aerospace Design (Springer Optimization and its applications)*, Vol. 66, Springer-Verlag London Limited, 2012.

[21] van Ginneken, D. A. J., Voskuijl, M., van Tooren, M. J. L., and Frediani, A., "Automated Control Surface Design and Sizing for the Prandtl Plane," *6th AIAA Multidisciplinary Design Optimization Specialist Conference*, 2010.

[22] Raju Kulkarni, A., Varriale, C., Voskuijl, M., La Rocca, G., and Veldhuis, L. L. M., "Assessment of Sub-scale Designs for Scaled Flight Testing," *AIAA Aviation Forum and Exposition*, American Institute of Aeronautics and Astronautics, 2019.

[23] Durham, W., Bordignon, K. A., and Beck, R., *Aircraft Control Allocation*, John Wiley & Sons, Ltd, 2016.

[24] Oppenheimer, M. W., Doman, D. B., and Bolender, M. A., "Control Allocation for Over-actuated Systems," *14th Mediterranean Conference on Control and Automation*, 2006.

Downloaded by TU DELFT on July 11, 2019 | http://arc.aiaa.org | DOI: 10.2514/6.2019-3001